Received: 14 June 2023 | Revised: 28 June 2023 | Accepted: 30 June 2023

DOI: 10.1002/pamm.202300013

RESEARCH ARTICLE

Characterisation of damage by means of electrical measurements: Numerical predictions

Dilek Güzel[1] | **Tobias Kaiser**[1] | **Lukas Lücker**[2] | **Nikolas Baak**[2] | **Frank Walther**[2] | **Andreas Menzel**[1,3]

[1]Institute of Mechanics, TU Dortmund University, Dortmund, Germany

[2]Materials Test Engineering, TU Dortmund University, Dortmund, Germany

[3]Division of Solid Mechanics, Lund University, Lund, Sweden

Correspondence
Dilek Güzel, Institute of Mechanics, TU Dortmund University,
Leonhard-Euler-Str. 5, 44227 Dortmund, Germany.
Email: dilek.guezel@tu-dortmund.de

[Correction added on 08 September 2023, after first online publication: Projekt DEAL funding statement has been added.]

Funding information
Deutsche Forschungsgemeinschaft, Grant/Award Number: 278868966

Abstract

Understanding damage mechanisms and quantifying damage is important in order to optimise structures and to increase their reliability. To achieve this goal, experimental- and simulation-based techniques are to be combined. Different methods exist for the analysis of damage phenomena such as fracture mechanics, phase field models, cohesive zone formulations and continuum damage modelling. Assuming a typical $[1-d]$-type damage formulation, the governing equations of continua that account for gradient-enhanced ductile damage under mechanical and electrical loads are derived. The mechanical and electrical sub-problems give rise to the local form of the balance equation of linear momentum, the micromorphic balance relation and the continuity equation for the electric charge, respectively. Experimental investigations indicate that changes in electrical conductivity arise due to the evolution of the underlying microstructure, for example, of cracks and dislocations. Therefore, motivated by deformation-induced property changes, the effective electrical conductivity is assumed to be a function of the damage variable. This eventually allows the prediction of experimentally recorded changes in the electrical resistance due to mechanically-induced damage processes. Interpreting the resistivity as a fingerprint of the material microstructure, the simulation approach proposed in the present work contributes to the development of non-destructive electrical-resistance-based characterisation methods. To demonstrate the applicability of the proposed framework, different representative simulations are studied.

KEYWORDS
ductile damage, electrical conductors, electro-mechanical coupling, finite element modelling

1 | INTRODUCTION

Ferrite/martensite dual-phase (DP) steels have been the focus of research and industrial applications over the past decades. DP steels are attractive materials for automotive-related sheet forming applications since they have high ultimate tensile strength, high ductility, high initial strain hardening rates and macroscopically homogenous plastic flow [1, 2]. These property enhancements are achieved by ferritic and martensitic constituents. However, the combination of ferritic and martensitic constituents also leads to the nucleations of voids, martensite cracking and decohesion of phase or grain boundaries due to the strong contrast of the constituents when undergoing plastic deformations [3]. Therefore, understanding the damage mechanisms and quantifying the damage is important in order to optimise structures and to increase their reliability.

Continuum damage mechanics denote a collection of approaches and models focusing on the simulation of degradation phenomena in continua. In these approaches, specific microstructural features and their evolution are not resolved – rather, the effect of the underlying microstructure on the material response is modelled. Different damage mechanisms such as microcracks, cracks along grain boundaries, growth of voids, rupture and decohesion are thus cumulatively taken into account. In order to model ductile damage, different approaches, namely micromechanically motivated and phenomenological damage models, have been the focus of research for the last 40 years.

Micromechanically motivated models take into account the underlying microstructure of the material and the specific damage mechanisms. On the other hand, phenomenological models describe the behaviour of a material based on macroscopic observations, without considering the underlying mechanisms. To this end, a scalar-valued damage variable d or a tensorial one $\boldsymbol{d}$ is introduced. In Lemaitre-type models, often referred to as $[1-d]$ models, damage is modelled as the degradation of elasticity and plasticity related quantities. Due to degradation and softening effects, the underlying mathematical problem is not well-posed. This manifests itself in a spurious mesh-dependency of finite element-based simulations. In order to overcome the loss of ellipticity of the governing equation, different regularisation approaches have been proposed. Regularisation can, for instance, be achieved by non-local damage models [4, 5], gradient-enhanced (micromorphic) approaches [6–9] and rate-dependent formulations for the damage evolution [10, 11].

The present contribution focuses on the characterisation of damage in ductile materials through electrical measurements. Changes in electrical conductivity can result from geometrical contributions and the underlying microstructure, for example, cracks [12, 13] or dislocations [14, 15]. In order to distinguish the individual effects of geometry change and microstructure, an electro-mechanically coupled framework, which considers the effect of plasticity and damage on electrical quantities, is established. More specifically speaking, the phenomenological model developed for the simulation of ductile damage in metallic materials and calibrated for DP800 steel by Sprave and Menzel [16] serves as a basis and is extended to electro-mechanical coupling in the present work. Motivated by experimental findings that indicate changes in conductivity under tensile loadings, the research question reads: *Can damage in DP800 steel be distinctly detected by means of electrical measurements and be predicted by means of simulations?* Figure 1 illustrates the change in conductivity due to various distinct effects and shows the experimental setup.

2 | CONTINUUM THERMODYNAMICS

Let nonlinear deformation map $\boldsymbol{\varphi}(\boldsymbol{X}, t)$ describe the deformation of body $\mathcal{B}$ and relate the position of a particle in the reference configuration $\boldsymbol{X} \in \mathcal{B}_0$ to its position in the spatial configuration $\boldsymbol{x} \in \mathcal{B}_t$ at time t. The associated tangent mapping is $\boldsymbol{F} = \partial\boldsymbol{\varphi}(\boldsymbol{X}, t)/\partial\boldsymbol{X}$ and it is observed that $J_F = \det(\boldsymbol{F}) > 0$ holds. Under quasi-static conditions, the mechanical sub-problem is governed by the balance equation of linear momentum in referential form

$$\nabla_{\boldsymbol{X}} \cdot \boldsymbol{P} = \boldsymbol{0} \qquad \forall \boldsymbol{X} \in \mathcal{B}_0 \tag{1}$$

whereby body forces are neglected. The free energy density Ψ serves as a potential for the Piola stress tensor, i.e.

$$\boldsymbol{P} = \frac{\partial \Psi}{\partial \boldsymbol{F}}. \tag{2}$$

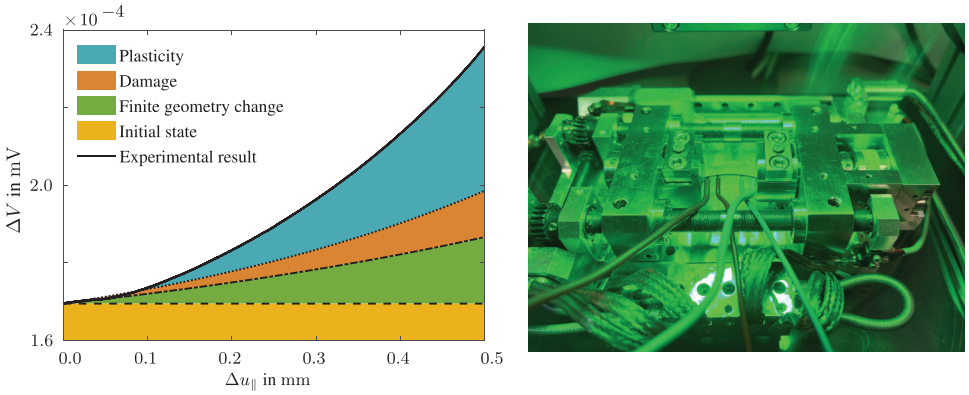

FIGURE 1 Left: Expected (microstructural) contributions to the overall change in the measured electric potential difference under tensile loadings and an applied constant current. The measured change in voltage ΔV with respect to applied transverse displacement $\Delta u_{\parallel}$ is illustrated. Right: The experiments are carried out with a micro-tensile machine (Kammrath & Weiß, 10-kN load cell). The resistance measurements are carried out with a nanovoltmeter (Keithley 2182A).

The representation of Piola stress tensor $\boldsymbol{P}$ in terms of Cauchy stress tensor $\boldsymbol{\sigma}$ is given as

$$\boldsymbol{P} = J_{\boldsymbol{F}}\, \boldsymbol{\sigma} \cdot \boldsymbol{F}^{-\mathrm{t}}. \tag{3}$$

In the micromorphic approach considered, the additional global degree-of-freedom $\phi(\boldsymbol{X}, t)$ is introduced for the regularisation of the damage formulation and stipulates the micromorphic balance relation

$$\nabla_{\boldsymbol{X}} \cdot \boldsymbol{Y} + Y = 0 \qquad \forall \boldsymbol{X} \in \mathcal{B}_0 \tag{4}$$

wherein flux $\boldsymbol{Y}$ and source term Y can be identified as

$$\boldsymbol{Y} = \frac{\partial \Psi}{\partial \nabla_{\boldsymbol{X}} \phi}, \quad Y = -\frac{\partial \Psi}{\partial \phi}. \tag{5}$$

Analogously, these quantities can be represented in terms of their spatial counterparts

$$\boldsymbol{Y} = J_{\boldsymbol{F}}\, \boldsymbol{F}^{-1} \cdot \boldsymbol{y}, \quad Y = J_{\boldsymbol{F}}\, y. \tag{6}$$

For (quasi-)stationary processes, the electrical sub-problem is governed by the continuity equation of electric charge which takes the referential form

$$\nabla_{\boldsymbol{X}} \cdot \boldsymbol{J} = 0 \qquad \forall \boldsymbol{X} \in \mathcal{B}_0 \tag{7}$$

and by Faraday's law of induction

$$\nabla_{\boldsymbol{X}} \times \boldsymbol{E} = \boldsymbol{0} \qquad \forall \boldsymbol{X} \in \mathcal{B}_0 \tag{8}$$

which can naturally be fulfilled by the introduction of a scalar-valued electric potential field V for the referential, $\boldsymbol{E} = -\nabla_{\boldsymbol{X}} V$, and spatial electric field vectors, $\boldsymbol{e} = -\nabla_{\boldsymbol{x}} V$. The spatial representations of the electric current density vector $\boldsymbol{j}$ and electric field vector $\boldsymbol{e}$ are related to their referential counterparts as

$$\boldsymbol{J} = J_{\boldsymbol{F}}\, \boldsymbol{F}^{-1} \cdot \boldsymbol{j}, \quad \boldsymbol{E} = \boldsymbol{F}^{\mathrm{t}} \cdot \boldsymbol{e}. \tag{9}$$

For the electrical conductors under investigation, it can be observed that the constitutive relation between the electric current density and the electric field is not derived from a potential but rather restricted by a Fourier-type inequality.

3 | CONSTITUTIVE RELATIONS

This section addresses the constitutive relations that are employed in the current work. In particular, the multi-surface ductile damage model proposed in [16] is briefly recapitulated in Section 3.1 and its extension to electro-mechanically coupled problems is discussed in Section 3.2.

3.1 | A multi-surface ductile damage model

The mechanical response is assumed to be governed by the volume-specific Helmholtz free energy density function Ψ. Specifically speaking, an additive decomposition according to

$$\Psi(\boldsymbol{F}, \boldsymbol{F}^{\mathrm{p}}, \phi, \nabla_{\boldsymbol{X}}\phi, d, \alpha) = \Psi^{\mathrm{loc}}(\boldsymbol{F}, \boldsymbol{F}^{\mathrm{p}}, d, \alpha) + \Psi^{\mathrm{nl}}(\boldsymbol{F}, \phi, \nabla_{\boldsymbol{X}}\phi, d) \tag{10}$$

is assumed with the local Ψ^{loc} and non-local Ψ^{nl} parts. In (10), d denotes the local damage variable, $\boldsymbol{F}^{\mathrm{p}} = [\boldsymbol{F}^{\mathrm{e}}]^{-1} \cdot \boldsymbol{F}$ represents the plasticity-related part of the deformation gradient and α characterises accumulated plastic strain.

The gradient-enhancement is incorporated into the model by means of the gradient of global damage variable ϕ in order to avoid the treatment of Karush–Kuhn–Tucker conditions on global finite element level. The non-local part can be specified as

$$\Psi^{\mathrm{nl}}(\boldsymbol{F}, \phi, \nabla_{\boldsymbol{X}}\phi, d) = \frac{c_d}{2}\|\nabla_{\boldsymbol{X}}\phi\|^2 + \frac{\beta_d}{2}[\phi - d]^2 \tag{11}$$

where c_d denotes a regularisation parameter and where β_d is a penalty parameter penalising deviations between the local and non-local damage variables. A constant regularisation parameter controlling the width of the localisation zone is chosen in the present contribution.

The local part of the energy function is formulated in terms of logarithmic strains $\boldsymbol{\varepsilon}^{\mathrm{e}} = \frac{1}{2}\ln(\boldsymbol{b}^{\mathrm{e}})$, with $\boldsymbol{b}^{\mathrm{e}} = \boldsymbol{F}^{\mathrm{e}} \cdot [\boldsymbol{F}^{\mathrm{e}}]^{\mathrm{t}}$ denoting the elastic left Cauchy–Green tensor. By noting that $\boldsymbol{b}^{\mathrm{e}}$ admits the spectral decomposition

$$\boldsymbol{b}^{\mathrm{e}} = \boldsymbol{F}^{\mathrm{e}} \cdot [\boldsymbol{F}^{\mathrm{e}}]^{\mathrm{t}} = \sum_{i=1}^{3} \left[\lambda_i^{\mathrm{e}}\right]^2 \boldsymbol{n}_i \otimes \boldsymbol{n}_i \tag{12}$$

the logarithmic strain tensor can be specified in terms of elastic principal stretches λ_i^{e} and eigendirection $\boldsymbol{n}_i$ as

$$\boldsymbol{\varepsilon}^{\mathrm{e}} = \sum_{i=1}^{3} \varepsilon_i^{\mathrm{e}}\, \boldsymbol{n}_i \otimes \boldsymbol{n}_i \quad \text{with} \quad \varepsilon_i^{\mathrm{e}} = \ln\left(\lambda_i^{\mathrm{e}}\right). \tag{13}$$

Moreover, volumetric and isochoric logarithmic strains can be obtained as

$$\varepsilon^{\mathrm{e,vol}} = \sum_{i=1}^{3} \varepsilon_i^{\mathrm{e}}, \quad \boldsymbol{\varepsilon}^{\mathrm{e,iso}} = \sum_{i=1}^{3} \left[\varepsilon_i^{\mathrm{e}} - \tfrac{1}{3}\varepsilon^{\mathrm{e,vol}}\right] \boldsymbol{n}_i \otimes \boldsymbol{n}_i. \tag{14}$$

The local part of the Helmholtz free energy density function,

$$\Psi^{\mathrm{loc}}(\boldsymbol{F}, \boldsymbol{F}^{\mathrm{p}}, d, \alpha) = \Psi^{\mathrm{loc,iso}}(\boldsymbol{\varepsilon}^{\mathrm{e}}, d) + \Psi^{\mathrm{loc,vol}}(\boldsymbol{\varepsilon}^{\mathrm{e}}, d) + \Psi^{\mathrm{loc,p}}(\alpha), \tag{15}$$

is defined by the volumetric, isochoric and hardening contribution

$$\Psi^{\mathrm{loc,vol}}(\boldsymbol{\varepsilon}^{\mathrm{e}}, d) = f^{\mathrm{vol}}(d)\frac{K}{2}\left[\varepsilon^{\mathrm{e,vol}}\right]^2 \tag{16a}$$

$$\Psi^{\mathrm{loc,iso}}(\boldsymbol{\varepsilon}^{\mathrm{e}}, d) = f^{\mathrm{iso}}(d) G\, \boldsymbol{\varepsilon}^{\mathrm{e,iso}} : \boldsymbol{\varepsilon}^{\mathrm{e,iso}} \tag{16b}$$

$$\Psi^{\mathrm{loc,p}}(\alpha) = \frac{h}{n_{\mathrm{p}} + 1}\, \alpha^{n_{\mathrm{p}}+1} \tag{16c}$$

with bulk modulus K, shear modulus G and with h and n_{p} controlling the hardening behaviour. In (16), f^{vol} and f^{iso} are exponentially decaying damage functions $f^{\bullet} : \mathbb{R}_0^+ \to (0, 1]$ defined by

$$f^{\bullet}(d) = \exp(-\eta\, \xi_{\bullet}\, d) \quad \text{with} \quad d \in [0, \infty) \tag{17}$$

where $\eta\, \xi_{\bullet}$ can be interpreted as the rate of degradation of effective material properties. Following standard procedures, the evaluation of the dissipation inequality results in the thermodynamic driving forces,

$$\boldsymbol{m}^{\mathrm{t}} = 2\, \frac{\partial \Psi}{\partial \boldsymbol{b}^{\mathrm{e}}} \cdot \boldsymbol{b}^{\mathrm{e}}, \quad q = -\frac{\partial \Psi}{\partial d}, \quad \beta = -\frac{\partial \Psi}{\partial \alpha}, \tag{18}$$

namely, the (spatial) Mandel stresses $\boldsymbol{m}^{\mathrm{t}}$, damage driving force q and isotropic hardening stress β. A multi-surface formulation that allows plasticity and damage to evolve based on potentials is adopted as

$$\phi^{\mathrm{p}}(\boldsymbol{m}^{\mathrm{t}}, \beta) = \left\| \mathrm{dev}\left(\frac{\boldsymbol{m}^{\mathrm{t}}}{f^{\mathrm{m}}(d)} \right) \right\| - \sqrt{\frac{2}{3}} [\sigma_{\mathrm{y0}} - \beta], \tag{19a}$$

$$\phi^{\mathrm{d}}(q, d) = \frac{q}{f^{\alpha}(\alpha)} - q_{\mathrm{max}}[1 - f^{\mathrm{q}}(\alpha)]^{n_{\mathrm{d}}}, \tag{19b}$$

where σ_{y0} corresponds to the initial yield stress and q_{max} is the threshold value for the driving force.

The plastic dissipation potential is formulated in terms of effective Mandel stresses by taking a damage function f^{m} into account. It resembles a classic von Mises-type yield function with isotropic hardening. For the damage dissipation potential, similar to the Mandel stresses, a function f^{q} is introduced by analogy to the damage functions and the damage dissipation potential is defined in terms of an effective damage driving force. Adopting an associative format yields the evolution equations for the internal variables and the corresponding Karush–Kuhn–Tucker conditions, i.e.

$$\lambda_{\mathrm{d}}\, \phi^{\mathrm{d}} = 0 \quad \text{with} \quad \phi^{\mathrm{d}} \leq 0, \quad \lambda_{\mathrm{d}} \geq 0 \tag{20a}$$

$$\lambda_{\mathrm{p}}\, \phi^{\mathrm{p}} = 0 \quad \text{with} \quad \phi^{\mathrm{p}} \leq 0, \quad \lambda_{\mathrm{p}} \geq 0 \tag{20b}$$

that are locally enforced with an active set method.

3.2 | Electrical subproblem

In accordance with the restrictions posed by the dissipation inequality ($\boldsymbol{j} \cdot \boldsymbol{e} \geq 0$, respectively $\boldsymbol{J} \cdot \boldsymbol{E} \geq 0$), the linear relation

$$\boldsymbol{j} = \boldsymbol{S}_t \cdot \boldsymbol{e} \tag{21}$$

between the spatial electric field vector and the spatial electric current density vector is assumed where $\boldsymbol{S}_t$ denotes the (positive semi-definite) spatial conductivity tensor. In virtue of (9), the electric current density vector $\boldsymbol{J}$ in the referential configuration can be obtained as

$$\boldsymbol{J} = J_{\boldsymbol{F}} \boldsymbol{F}^{-1} \cdot \boldsymbol{S}_t \cdot \boldsymbol{F}^{-\mathrm{t}} \cdot \boldsymbol{E}. \tag{22}$$

In order to study the effect of geometry changes on the electrical problem, the constant spatial conductivity tensor

$$\boldsymbol{S}_t = \kappa_t\, \boldsymbol{I}, \tag{23}$$

defined in terms of the scalar-valued conductivity parameter $\kappa_t > 0$, is taken as a reference. In the presence of damage, accumulated dislocations or other distinct microstructural effects, the electrical conductivity is expected to decrease, similar to elastic properties. In this case, the electrical conductivity tensor is assumed to be of the form

$$\boldsymbol{S}_t = g^{\mathrm{V}}(d, \alpha) \kappa_t\, \boldsymbol{I} \quad \text{with} \quad g^{\mathrm{V}} : \mathbb{R}_0^+ \times \mathbb{R}_0^+ \to (0, 1] \tag{24}$$

where g^{V} defines the decay in electrical conductivity.

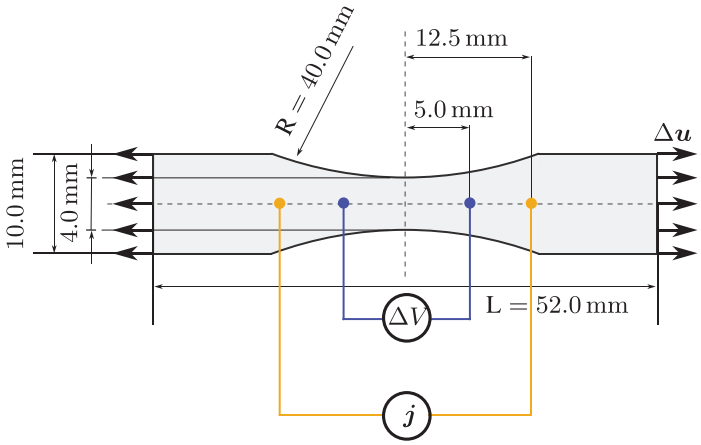

E	207.00 GPa	ν	0.2100
σ_{y0}	258.59 MPa	h	1705.64 MPa
n_p	0.2654	q_{max}	0.6953 MPa
n_d	0.6667	η	0.1559
ξ_{vol}	1.0000	ξ_{iso}	0.5861
ξ_q	0.8100	ξ_m	0.6163
η_α	0.0000	c_d	0.5400 N
β_d	500.00 MPa	κ_t	4016.1 A/[Vmm]

FIGURE 2 Geometrical dimensions of the micro-tensile sample and boundary conditions of the boundary value problem discussed in Section 4. The thickness of the sample is 1.5 mm. Material parameters are identified for DP800 steel for the material model that is introduced in Section 3.1, cf. [16].

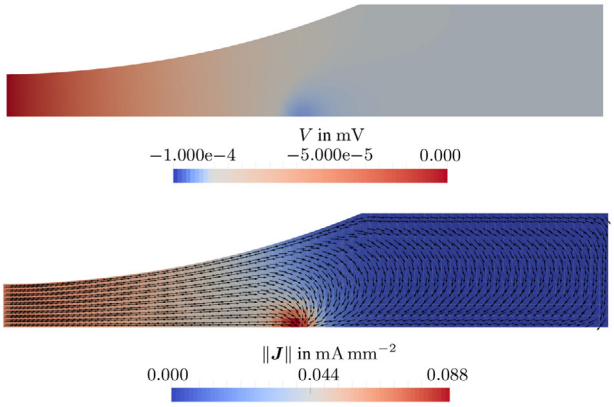

FIGURE 3 Top: Electric potential field in the midplane of the symmetric boundary value problem depicted in Figure 2 for $\Delta \boldsymbol{u}_{\parallel} = 0.5$ mm and applied electric current density $I = 0.4$ A. Damage and plasticity parameters for the electrical subproblem are chosen as $\chi_d = 0.01, \chi_\alpha = 0.20$. Bottom: Electric current density field $\|\boldsymbol{J}\| = \sqrt{\boldsymbol{J} \cdot \boldsymbol{J}}$ in the midplane. Electric current density vectors are indicated by black arrows.

4 | NUMERICAL EXAMPLES

In this section, the modelling approach proposed in Section 3 is applied to the boundary value problem depicted in Figure 2, which mimics the Direct Current Potential Drop (DCPD) measurements. The measurements in Figure 1 are obtained while the specimen is subjected to tensile loading. Voltage measurements are collected with constant current $I = 0.8$ A being applied between the contact points throughout the experiment [17, 18]. The material parameters that are identified for DP800 steel are given in Figure 2. In the un-deformed state, the initial resistivity $R = 0.249\,\Omega\,\text{mm}^2$ of the DP800 sheet metal, corresponding to the initial conductivity $\kappa_t = 4016.1$ A/[Vmm], was experimentally determined. The damage function controlling the degradation of electrical properties is chosen as

$$g^{\mathrm{V}}(d, \alpha) = \exp\left(-\chi_d\, d - \chi_\alpha\, \alpha\right) \tag{25}$$

such that damage and accumulated plastic strain affect the electrical conductivity. The parameters χ_d and χ_α can be identified based on voltage measurements. By using symmetries, the electric potential and electric current density fields are visualised in Figure 3 for the tensile specimen given in Figure 2.

Figure 4 illustrates three distinct cases. For the first case ($\chi_d = 0, \chi_\alpha = 0$), the electrical conductivity is assumed to be constant. This assumption allows the study of the influence of finite geometry changes on the measured electric

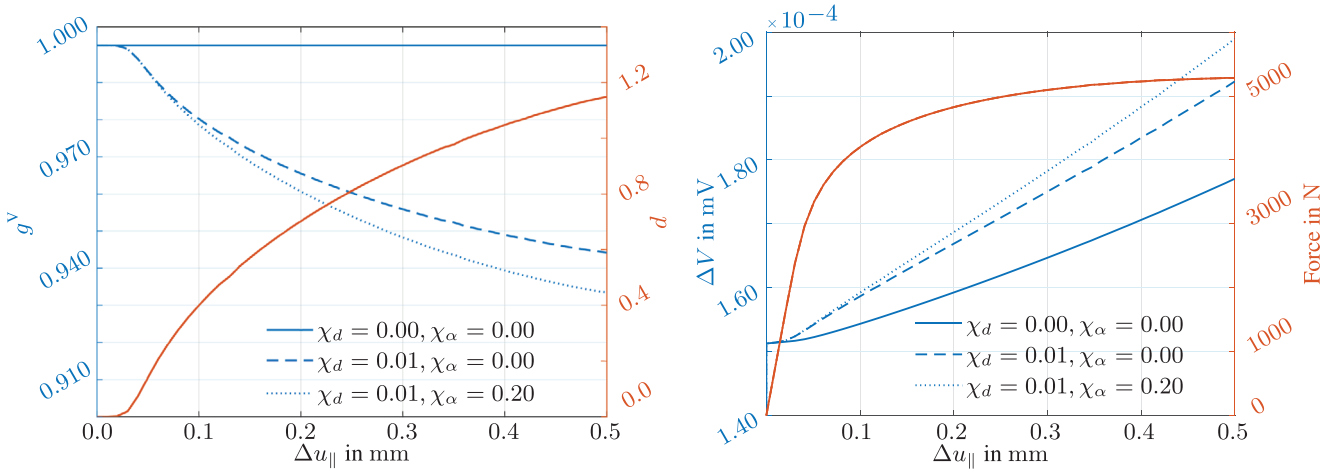

FIGURE 4 Left: Evolution of local damage variable at the point of voltage measurements, as illustrated in Figure 2 and corresponding damage function controlling the degradation of electrical properties. The parameters χ_d and χ_α can be interpreted as the rate of degradation of electrical conductivity due to damage and plasticity, respectively. Right: Electric potential difference at the point of voltage measurement. Reaction force–displacement diagram of the tensile test for three distinct cases showing an identical response.

potential field while keeping a constant applied electric current. In other words, this corresponds to the case that the influence of various microstructural effects (e.g. the evolution of damage and plasticity) on the electrical conductivity is neglected. Motivated by experimental findings that indicate a decrease in the conductivity with increasing dislocation density and damage [12, 14, 15], the set of parameters ($\chi_d = 0.01, \chi_\alpha = 0.20$) is chosen for the second study. Clearly, both the evolution of damage and plasticity affect the electrical conductivity in this case. Finally, consider the case where only damage accumulation is assumed to have an effect on the electrical conductivity, such that ($\chi_d = 0.01, \chi_\alpha = 0$). From a physics point of view, this corresponds to a dislocation free state that can be obtained with an appropriate heat treatment. The previous study exemplifies that the influence of different microscale processes and of geometry changes can be well-distinguished in simulations. Such a distinction is rather difficult to achieve in experiments but required for the development of non-destructive testing methods. As indicated in Figure 4, the mechanical response in the form of reaction forces or accumulated damage is not influenced by the electrical sub-problem.

5 | CONCLUSION

Motivated by the change in electrical conductivity due to finite geometry changes, dislocation density and mechanically-induced damage, this contribution focuses on an electro-mechanically coupled ductile damage formulation for metals, specifically DP800 steel. Experimental findings show that various mechanisms may influence the electrical conductivity. In order to support the non-destructive electrical characterisation of damage, these mechanisms should be taken into account. The proposed framework allows the separation of individual contributions as demonstrated in the present study based on representative simulation results. In this regard, it is important to note that the constitutive relations for the electrical subproblem are purely academic at this stage and are not based on experimental data. The application to experiments will, accordingly, be the focus of future works.

ACKNOWLEDGMENTS

Funded by the Deutsche Forschungsgemeinschaft (DFG, German Research Foundation) – Project-ID 278868966 – TRR 188.
Open access funding enabled and organized by Projekt DEAL.

ORCID

Dilek Güzel https://orcid.org/0000-0001-7461-8549
Tobias Kaiser https://orcid.org/0000-0002-1979-1944
Andreas Menzel https://orcid.org/0000-0002-7819-9254

REFERENCES

1. Tasan, C., Diehl, M., Yan, D., Bechtold, M., Roters, F., Schemmann, L., Zheng, C., Peranio, N., Ponge, D., Koyama, M., Tsuzaki, K., & Raabe, D. (2015). An overview of dual-phase steels: Advances in microstructure-oriented processing and micromechanically guided design. *Annual Review of Materials Research*, *45*(1), 391–431.
2. Kalhor, A., Taheri, A. K., Mirzadeh, H., & Uthaisangsuk, V. (2021). Processing, microstructure adjustments, and mechanical properties of dual phase steels: A review. *Materials Science and Technology*, *37*(6), 561–591.
3. Meya, R., Kusche, C. F., Löbbe, C., Al-Samman, T., Korte-Kerzel, S., & Tekkaya, A. E. (2019). Global and high-resolution damage quantification in dual-phase steel bending samples with varying stress states. *Metals*, *9*, 319.
4. Bažant, Z. P., & Pijaudier-Cabot, G. (1988). Nonlocal continuum damage, localization instability and convergence. *ASME Journal of Applied Mechanics*, *55*, 287–293.
5. Enakoutsa, K., Leblond, J., & Perrin, G. (2007). Numerical implementation and assessment of a phenomenological nonlocal model of ductile rupture. *Computer Methods in Applied Mechanics and Engineering*, *196*(13), 1946–1957.
6. Aifantis, E. C. (1987). The physics of plastic deformation. *International Journal of Plasticity*, *3*(3), 211–247.
7. Peerlings, R. H. J., Borst, R. D., Brekelmans, W. A. M., Vree, J. H. P. D., & Spee, I. (1996). Some observations on localisation in non-local and gradient damage models. *European Journal of Mechanics A: Solids*, *15*, 937–953.
8. Steinmann, P. (1999). Formulation and computation of geometrically non-linear gradient damage. *International Journal for Numerical Methods in Engineering*, *46*, 757–779.
9. Forest, S. (2009). Micromorphic approach for gradient elasticity, viscoplasticity, and damage. *Journal of Engineering Mechanics*, *135*(3), 117–131.
10. Duvant, G., John, C., & Lions, J. (2012). *Inequalities in Mechanics and Physics*, Grundlehren der mathematischen Wissenschaften. Springer.
11. Langenfeld, K., Junker, P., & Mosler, J. (2018). Quasi-brittle damage modeling based on incremental energy relaxation combined with a viscous-type regularization. *Continuum Mechanics and Thermodynamics*, *30*(5), 1125–1144.
12. Cordill, M. J., Glushko, O., & Putz, B. (2016). Electro-mechanical testing of conductive materials used in flexible electronics. *Frontiers in Materials*, *3*, 1–11.
13. Kaiser, T., Cordill, M., Kirchlechner, C., & Menzel, A. (2021). Electrical and mechanical behaviour of metal thin films with deformation-induced cracks predicted by computational homogenisation. *International Journal of Fracture*, *231*(2), 223–242.
14. Bishara, H., Tsybenko, H., Nandy, S., Muhammad, Q. K., Frömling, T., Fang, X., Best, J. P., & Dehm, G. (2022). Dislocation-enhanced electrical conductivity in rutile TiO2 accessed by room-temperature nanoindentation. *Scripta Materialia*, *212*, 114543.
15. Muhammad, Q., Bishara, H., Porz, L., Dietz, C., Ghidelli, M., Dehm, G., & Frömling, T. (2022). Dislocation-mediated electronic conductivity in rutile. *Materials Today Nano*, *17*, 100171.
16. Sprave, L., & Menzel, A. (2020). A large strain gradient-enhanced ductile damage model: Finite element formulation, experiment and parameter identification. *Acta Mechanica*, *231*(12), 5159–5192.
17. Koch, A., Bonhage, M., Teschke, M., Lücker, L., Behrens, B. A., & Walther, F. (2020). Electrical resistance-based fatigue assessment and capability prediction of extrudates from recycled field-assisted sintered EN AW-6082 aluminium chips. *Materials Characterization*, *169*, 110644.
18. Lücker, L., Lingnau, L., & Walther, F. (2022). Non-destructive direct current potential drop assessment of forming-induced pre-damage in AISI 5115 steel. *Procedia Structural Integrity*, *42*, 368–373.

How to cite this article: Güzel, D., Kaiser, T., Lücker, L., Baak, N., Walther, F., & Menzel, A. (2023). Characterisation of damage by means of electrical measurements: Numerical predictions. *Proceedings in Applied Mathematics and Mechanics*, *23,* e202300013. https://doi.org/10.1002/pamm.202300013